

Article

Structure-Based Virtual Screening of Furan-1,3,4-Oxadiazole Tethered *N*-phenylacetamide Derivatives as Novel Class of hTYR and hTYRP1 Inhibitors

Ali Irfan ¹, Shah Faisal ², Sajjad Ahmad ³, Sami A. Al-Hussain ⁴, Sadia Javed ⁵, Ameer Fawad Zahoor ^{1,*}, Bushra Parveen ¹ and Magdi E. A. Zaki ^{4,*}

¹ Department of Chemistry, Government College University Faisalabad, Faisalabad 38000, Pakistan

² Department of Chemistry, Islamia College University Peshawar, Peshawar 25120, Pakistan

³ Department of Health and Biological Sciences, Abasyn University, Peshawar 25000, Pakistan

⁴ Department of Chemistry, College of Science, Imam Mohammad Ibn Saud Islamic University (IMSIU), Riyadh 11623, Saudi Arabia

⁵ Department of Biochemistry, Government College University Faisalabad, Faisalabad 38000, Pakistan

* Correspondence: fawad.zahoor@gcuf.edu.pk (A.F.Z.); mezaki@imamu.edu.sa (M.E.A.Z.);

Tel.: +92-3336729186 (A.F.Z.)

Abstract: Human tyrosinase (hTYR) is a key and rate-limiting enzyme along with human tyrosinase-related protein-1 (hTYRP1), which are among the most prominent targets of inhibiting hyper pigmentation and melanoma skin cancer. In the current in-silico computer-aided drug design (CADD) study, the structure-based screening of sixteen furan-1,3,4-oxadiazole tethered *N*-phenylacetamide structural motifs **BF1–BF16** was carried out to assess their potential as hTYR and hTYRP1 inhibitors. The results revealed that the structural motifs **BF1–BF16** showed higher binding affinities towards hTYR and hTYRP1 than the standard inhibitor kojic acid. The most bioactive lead furan-1,3,4-oxadiazoles **BF4** and **BF5** displayed stronger binding in affinities (−11.50 kcal/mol and −13.30 kcal/mol) than the standard drug kojic acid against hTYRP1 and hTYR enzymes, respectively. These were further confirmed by MM-GBSA and MM-PBSA binding energy computations. The stability studies involving the molecular dynamics simulations also provided stability insights into the binding of these compounds with the target enzymes, wherein it was found that they remain stable in the active sites during the 100 ns virtual simulation time. Moreover, the ADMET, as well as the medicinal properties of these novel furan-1,3,4-oxadiazole tethered *N*-phenylacetamide structural hybrids, also showed a good prospect. The excellent in-silico profiling of furan-1,3,4-oxadiazole structural motifs **BF4** and **BF5** provide a hypothetical gateway to use these compounds as potential hTYRP1 and hTYR inhibitors against melanogenesis.

Keywords: furan-1,3,4-oxadiazole; hTYR; hTYRP1; melanogenesis; molecular docking; MD simulations



Citation: Irfan, A.; Faisal, S.; Ahmad, S.; Al-Hussain, S.A.; Javed, S.; Zahoor, A.F.; Parveen, B.; Zaki, M.E.A.

Structure-Based Virtual Screening of Furan-1,3,4-Oxadiazole Tethered *N*-phenylacetamide Derivatives as Novel Class of hTYR and hTYRP1 Inhibitors. *Pharmaceuticals* **2023**, *16*, 344. <https://doi.org/10.3390/ph16030344>

Academic Editors: Hasan Demirci, Halil Ibrahim Ciftci and Belgin Sever

Received: 30 December 2022

Revised: 10 February 2023

Accepted: 12 February 2023

Published: 23 February 2023



Copyright: © 2023 by the authors. Licensee MDPI, Basel, Switzerland. This article is an open access article distributed under the terms and conditions of the Creative Commons Attribution (CC BY) license (<https://creativecommons.org/licenses/by/4.0/>).

1. Introduction

Skin cancer is the one of the most common cancers which adversely affect humans. The main types of skin cancer include melanoma, basal cell carcinoma and squamous. Among them, melanoma is far less frequent than the other types. Melanoma cancer has a higher propensity to spread to other body areas by invading adjacent tissue [1]. Melanoma is the skin cancer that leads to the majority of fatalities, with an average increase of roughly one million new cases per year. Skin cancer has developed into the most prevalent malignant ailment, accounting for 4.5% of all new cancer cases, and it continues to be a fatal cancer that causes significant socioeconomic challenges [2–4]. When melanomas are in an advanced stage, they are required to be treated surgically and with adjuvant systemic therapies [5]. As with other malignancies, radiation can be used alone or in combination with surgery to treat melanoma. However, radiotherapy

has a limited function in the treatment of melanoma since it is radio-resistant in comparison to other malignancies [6]. Thus, the development of drugs that specifically target cell-signaling pathways involved in this malignancy holds promise for the treatment of melanomas [7,8]. The enzyme human tyrosinase (hTYR) and human tyrosinase-related protein-1 (hTYRP1) are involved in the biosynthetic processes that produce the pigment melanin in the melanocytes. The hTYR and hTYRP1 have been shown to be sensitive melanoma biomarkers and these are also overexpressed during carcinogenesis [9–11]. Additionally, the melanin biosynthesis pathway produces powerful immunosuppressive intermediate species such as L-DOPA and other reactive quinines which further aggravate melanomas by negating the anti-melanoma actions of the immunotherapeutic medications that target these malignancies [12–15].

All the observations and factors link the elevated melanogenesis as a cause of the lethality of skin melanomas due to the increased activity and overexpression of hTYR and hTYRP1 [13,16]. Therefore, targeting the inhibition of crucial enzymes hTYR and hTYRP1 with suitable inhibitors prevents the formation of melanomas and may help in treating these cancers [13,17,18]. To date, several approaches of in-vivo studies targeting the melanin biosynthetic pathway for treating melanomas have been reported [19]. hTYR, hTYRP1 and the other related enzymes of the melanin biosynthetic pathway are possible molecular targets in the treatment of melanoma and other melanogenesis-related disorders due to their overexpression, which occurs during carcinogenesis primarily in the melanocytes [13,20,21].

The plethora of literature cited in previous studies revealed that numerous furans containing molecules, benzofurans (Figure 1), 1,3,4-oxadiazoles (Figure 1), furan-1,3,4-oxadiazoles and other furan moiety carrying scaffolds are effective inhibitors of mushroom and human tyrosinases. The origin of furan chemistry has been outlined by Partington and the furan first derivative pyromucic acid (furan-2-carboxylic acid) or simply 2-furoic acid (Figure 1) was obtained via dry distillation of mucic acid (Figure 1). In 1831, Johann Wolfgang Döbereiner reported another important derivative of furan called furfural (Figure 1) (furan-2-carbaldehyde), which was further characterized by John Stenhouse. Heinrich Limpricht isolated furan for the first time in 1870 from pine wood, called tetraphenol due to the presence of four carbon atoms and strong resemblance to phenol in many reactions, e.g., with bromine [22–25].

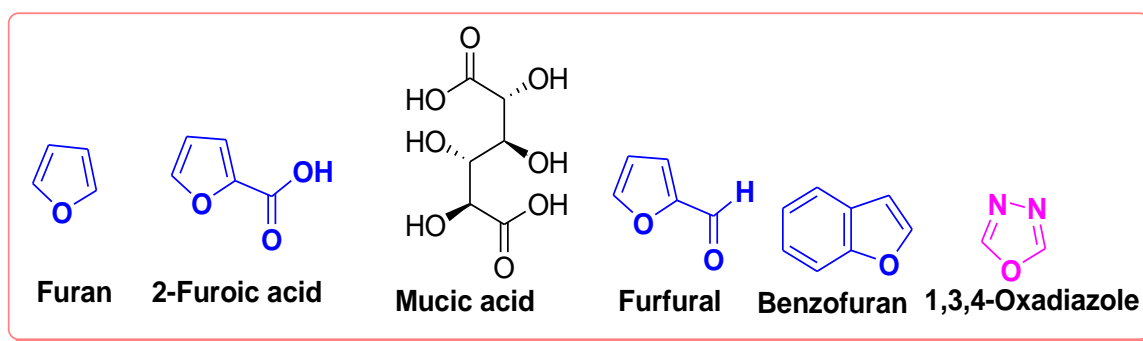


Figure 1. Structures of furan, mucic acid, 1,3,4-oxadiazole and furan-related compounds.

Furan, benzofuran and other nitrogen-oxygen heterocyclic structural motifs had demonstrated excellent medicinal and pharmacological profiles, and exhibited a wide spectrum of biological activities such as antibacterial, anti-fungal, anti-diabetic, anti-acetylcholine, anti-viral, anti-inflammatory, anti-parasitic, fluorescent sensor for analgesic, anti-HepG-2, anti-oxidative, bone anabolic agent and as bacterial tyrosinase inhibitors; they are also part of many natural and synthetic clinical drugs. In various research models, furan scaffolds have shown potent anti-tyrosinase actions which imply that these compounds are effective inhibitors of the melanin biosynthesis in the melanocytes and can be used

in treating skin melanomas and other melanogenesis-related disorders, as depicted in Figure 2 [26–38].

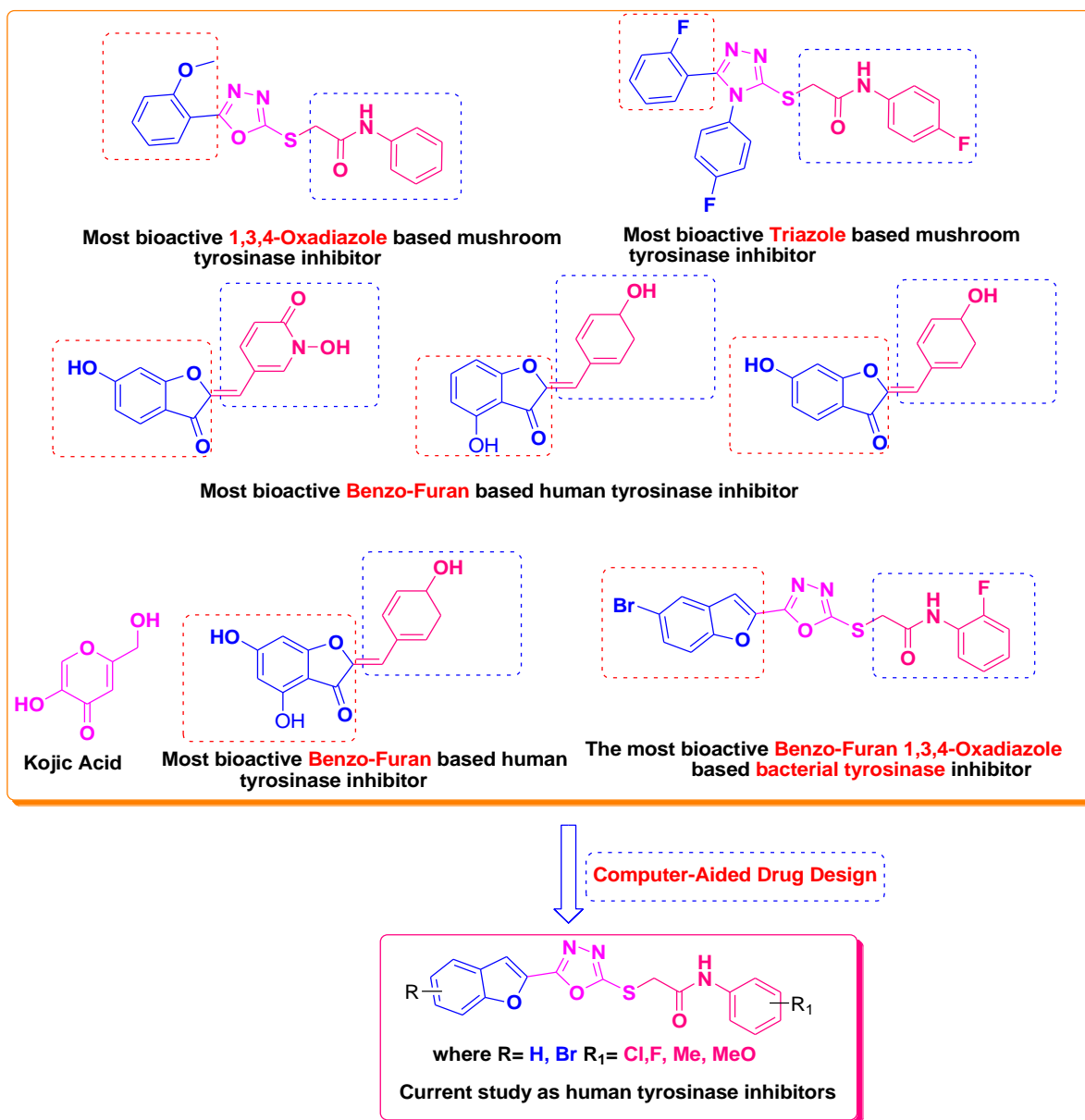


Figure 2. Bioactive tyrosinase inhibitors.

Our previous work reported the evaluation of benzofuran-1,3,4-oxadiazole tethered *N*-phenylacetamides as bacterial tyrosinase inhibitors and showed strong repressive activities of benzofuran compounds, which encouraged us to apply computer-aided drug discovery (CADD) approaches to assess the therapeutic potential of sixteen synthesized furan-1,3,4-oxadiazole tethered *N*-phenylacetamide structural hybrids, **BF1–BF16** [38,39], with different substituents to target the crucial enzymes hTYR and hTYRP1 of the melanin biosynthetic pathway.

The therapeutic potential of synthesized furan–oxadiazole scaffolds **BF1–BF16** was assessed utilizing a computer-aided drug design (CADD) workflow as displayed in Figure 3.

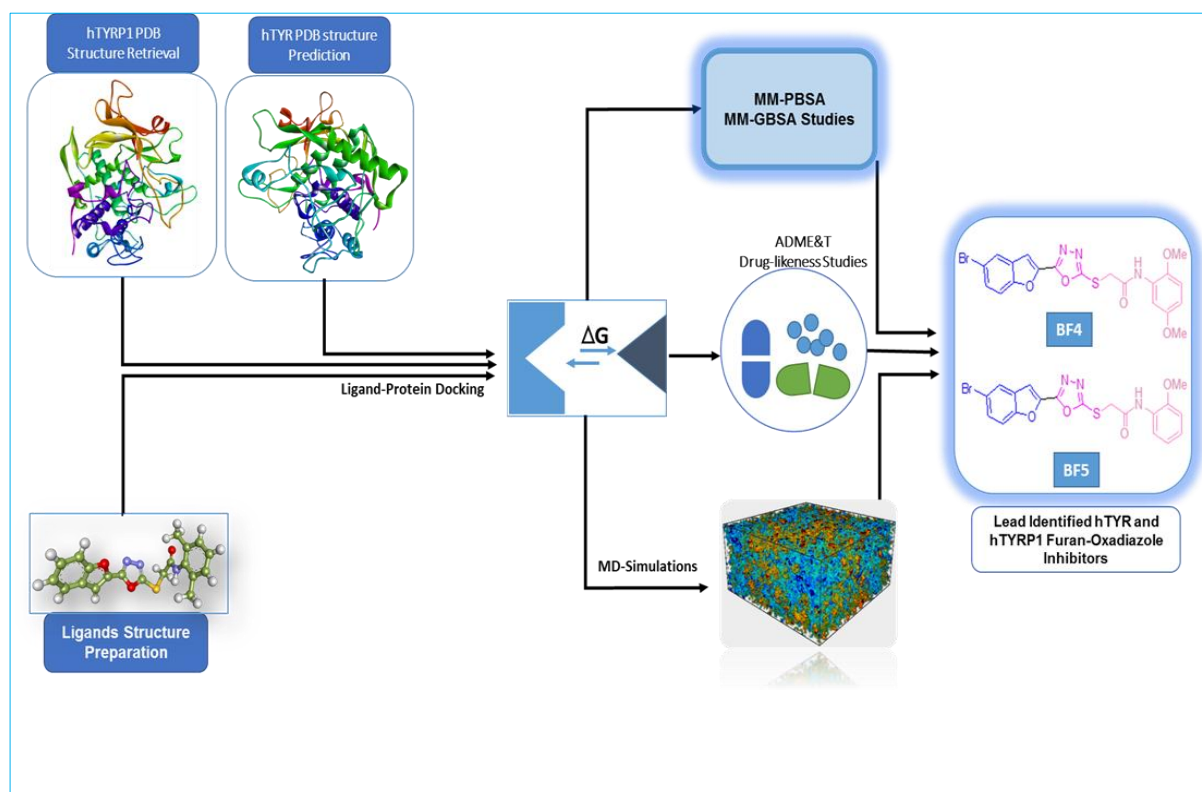


Figure 3. In silico work flow for discovery of novel hTYR and hTYRP1 inhibitors via CADD.

2. Results and Discussion

2.1. Computational Investigations of BF1–BF16 against hTYR and hTYRP1

Utilizing the in silico molecular docking approach, we evaluated furan-1,3,4-oxadiazoles synthesized compounds **BF1–BF16** using the molecular operating environment (MOE) against the hTYR and hTYRP1 of the melanin synthesis pathway and compared these results with the standard tyrosinase inhibitor drug kojic acid, which has been shown to repress these two enzymes (hTYR and hTYRP1) in various studies. The results of these investigations revealed that the anti-hTYR and hTYRP1 repressive agent kojic acid binds to the active site of the hTYR enzyme with a binding affinity score of -6.62 Kcal/mol, and it binds to the hTYRP1 with a binding affinity score of -8.90 Kcal/mol. Conformation analysis of the kojic acid inhibitor inside the active site pocket of hTYR revealed that it engaged multiple amino acids residues (ASN364, HIS367, and MET374) and made conventional-type and carbon–hydrogen-type hydrogen bonds with it; along with several other molecular interactions of Pi–Pi T-shaped and Pi–Alkyl-type interactions with HIS202 and VAL377 were also observed in the hTYR and kojic acid protein–ligand complex. Binding analysis of kojic acid with the hTYRP1 enzyme showed that it made conventional hydrogen bonds with the TYR362 and GLY389 active site residues and a Pi–Pi stacked interaction with the HIS381. The conformational poses of kojic acid with both enzymes are presented in Figure 4.

In comparison with the kojic acid inhibitor, some of the synthesized benzofuran compounds showed robust interactions and higher binding affinities with the hTYR and hTYRP1 enzymes of the melanin synthesis pathway. Out of the sixteen compounds, **BF1–BF16**, three compounds, **BF5**, **BF7**, and **BF15**, showed stronger affinities against the hTYR, while the other three, **BF4**, **BF5**, and **BF7**, showed stronger affinities against the hTYRP1 compared to the standard drug kojic acid. Analysis of the conformational pose and binding affinity of **BF5** showed that it binds to the hTYR active site with a binding affinity score of -13.30 Kcal/mol and forms multiple molecular interactions with the hTYR enzyme receptor residues. Hydrogen bonds of conventional and carbon–hydrogen types were

noted between the benzofuran ring of **BF5** and HIS202, HIS367, GLN376, MET374 residues. Moreover, other interactions, such as Pi–Anion, Alkyl, and Pi–Alkyl interactions (with the VAL377), were also present between the 1,3,4-oxadiazole and benzofuran rings of this compound; in addition, several of the hTyrosinase receptor residues (ASP186 and ARG196) also made halogen molecular interactions with the bromine present on the benzofuran ring of this compound. These are diagrammatically presented in Figure 5.

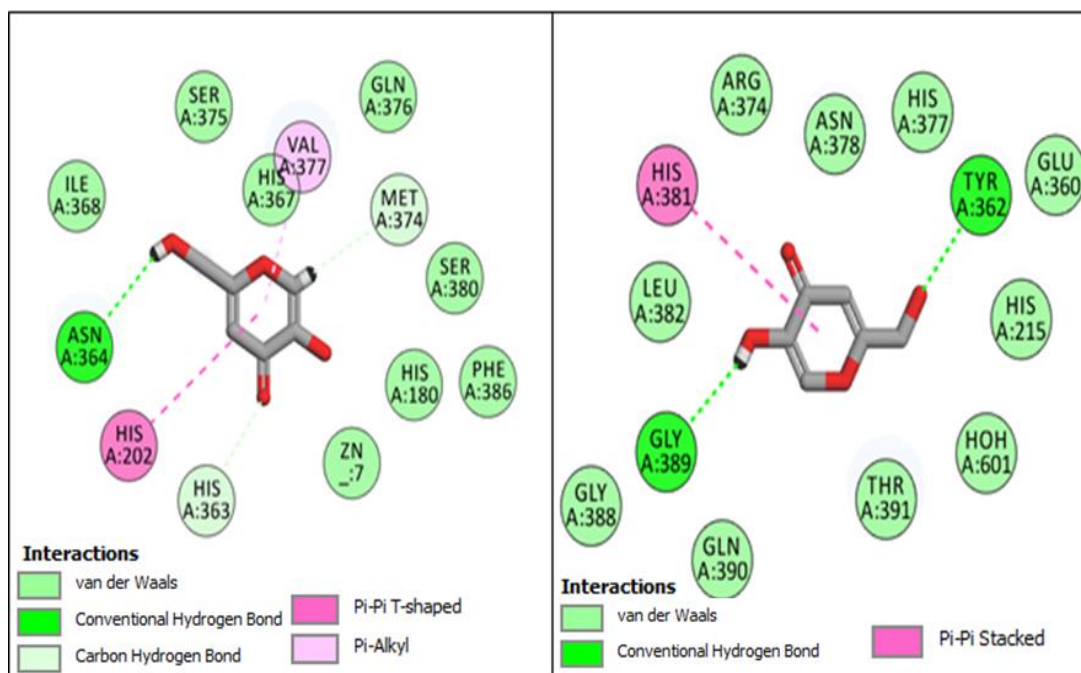


Figure 4. Conformational poses of kojic acid with hTYR (Left panel) and hTYRP1 (Right panel).

The two other compounds, **BF7** and **BF15**, were also able to bind to the hTyrosinase with higher binding affinities (−11.19 Kcal/mol and −11.88 Kcal/mol, respectively) compared to the kojic acid, which was able to bind to the hTYR with a binding affinity of −6.62 Kcal/mol. These two compounds were also able to engage multiple active site residues of hTYR via a different type of molecular interactions. Overall, the **BF7** compound showed a similar kind of binding conformation and interactions with the hTyrosinase enzyme; however, the sulfur atom of **BF7** made two more Pi–sulfur interactions with the HIS363, and HIS202 and the chlorine atom present on the phenyl ring of the **BF7** made two halogen interactions with the VAL377 and MET374 active site residues. Similarly, **BF15** also showed robust binding with the hTyrosinase by engaging the HIS363 with a carbon–hydrogen-type hydrogen bond, while PHE347 made a molecular contact via a Pi–sulfur interaction with the sulfur atom of **BF15**. Several other types of hydrophobic interactions were also observed between the benzofuran, 1,3,4-oxadiazole, and the phenyl ring of **BF15**, and they can be seen in Figure 6.

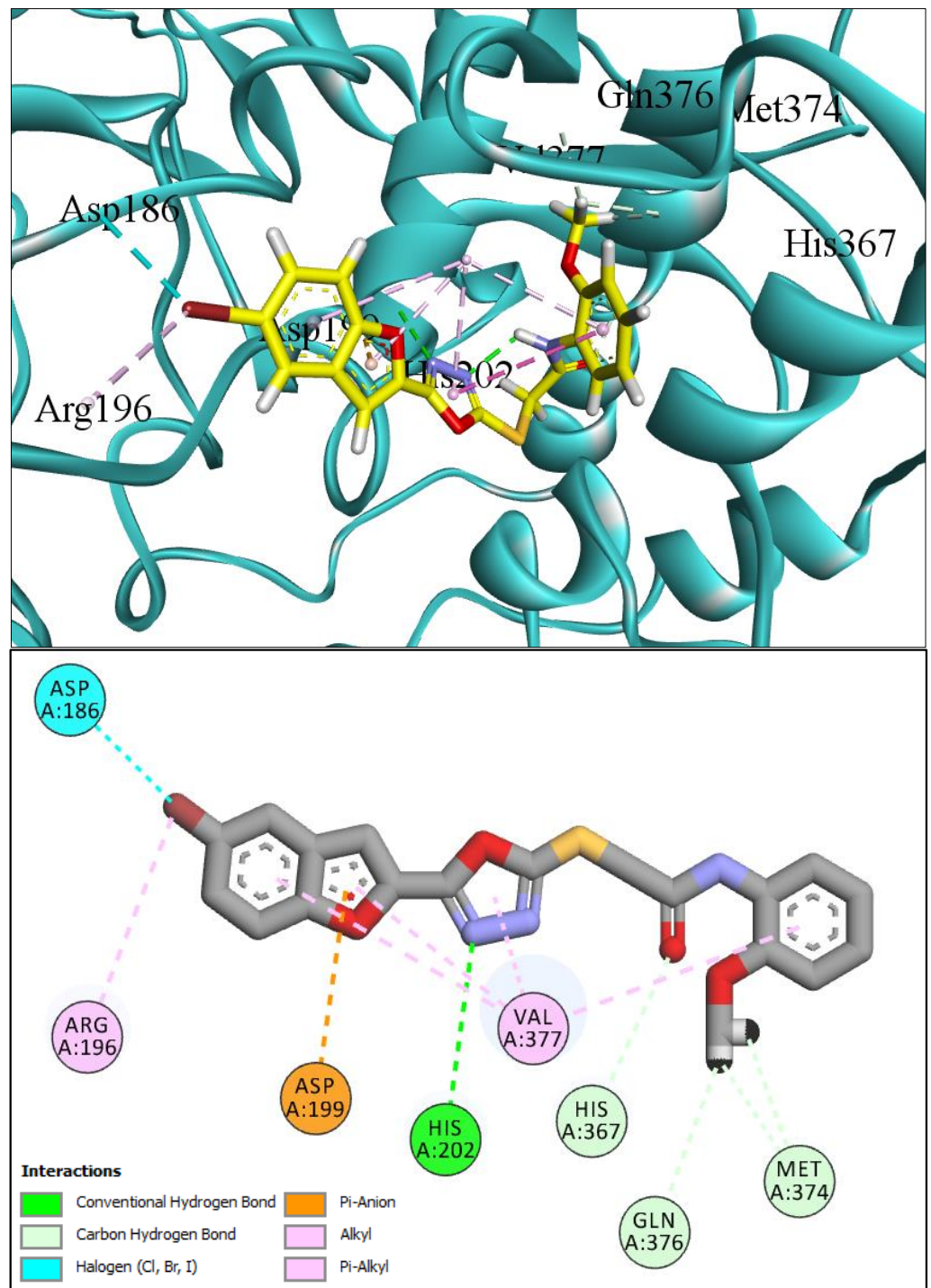


Figure 5. Three-dimensional conformational pose of BF5 with hTyrosinase (Upper panel) and two-dimensional pose (Lower panel).

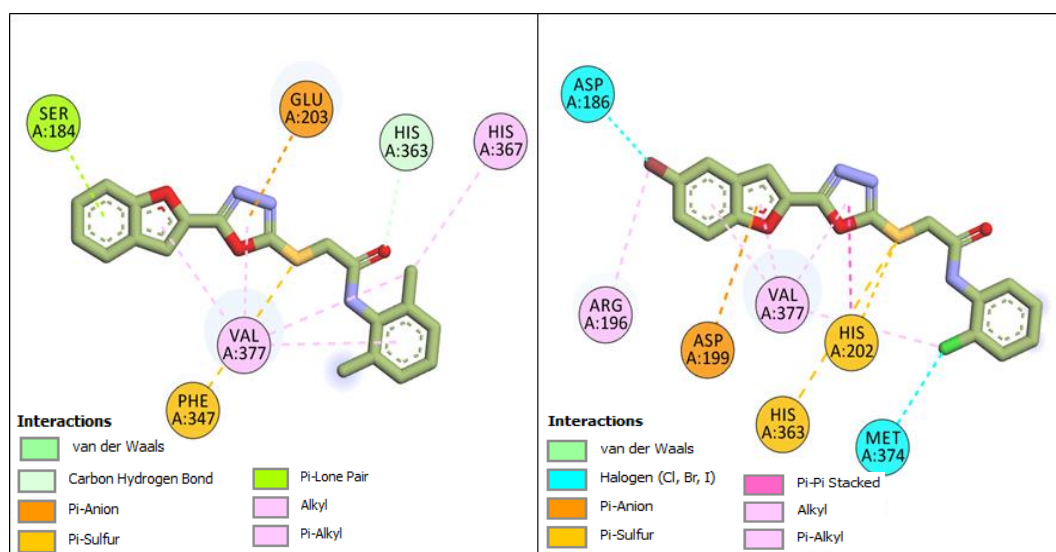


Figure 6. Two-dimensional conformational pose of **BF7** with hTyrosinase (**Right panel**) and two-dimensional conformational pose of **BF15** with hTyrosinase (**Left panel**).

The molecular docking investigations against the hTYRP1 enzyme also revealed that these newly synthesized compounds show superior binding and interactions with this important enzyme. The standard inhibitor kojic acid, as discussed in the previous paragraphs, binds to the hTYRP1 with a binding affinity score of -8.90 Kcal/mol; compared to kojic acid, some of these new furan-1,3,4-oxadiazoles (**BF4**, **BF5**, and **BF7**) have shown good binding affinities towards the hTYRP1 enzyme. The furan-1,3,4-oxadiazoles **BF4**, **BF5** and **BF7** were able to bind to the hTYRP1 with binding affinities of -11.50 Kcal/mol, -11.55 Kcal/mol, and -11.29 Kcal/mol, respectively. The conformational pose analysis of **BF4** in the active site of the hTYRP1 enzyme showed that it binds with the active pocket residues via different types of molecular interactions. The acetamide group, as well as the oxygen atom of the 1,3,4-oxadiazole ring present in this compound, made conventional hydrogen bonds with the ARG374 and THR391 amino acids of the hTYRP1, and a carbon-hydrogen-type H-bond between the $-OCH_3$ and the SER394 amino acid was also present in this ligand-protein complex. The 1,3,4-oxadiazole ring of **BF4** also made another Pi-anion interaction with the GLU216 of the hTYRP1 active site, while the bromine atom on the benzofuran ring and the phenyl ring of **BF-4** made Alkyl and Pi-Alkyl interactions with LEU293 and LYS198 residues of hTYRP1. **BF5**, which showed the highest binding affinity (-11.55 Kcal/mol) towards the hTYRP1 active site, also showed robust interactions of different types with this target enzyme. The phenyl ring of **BF-5** made a total of four interactions with the HIS381, GLN390, and HIS377 of Pi-Pi stacked, Pi-Pi T-shaped and amide-Pi stacked type along with a direct interaction with the zinc ion present in the active site of the hTYRP1. The 1,3,4-oxadiazole ring engaged the THR391 residue while the benzofuran ring made three Pi-anion interactions with the ASP212 and GLU216; however, the $-OCH_3$ present on the phenyl ring made a single carbon-hydrogen-type H-bond with the HIS215 of the hTYRP1 enzyme active site. Figure 7 shows the three and two-dimensional conformations of **BF5** inside the hTYRP1 active site.

The furan-1,3,4-oxadiazole **BF7** compound with a binding affinity of -11.29 Kcal/mol with the hTYRP1 also exhibited several different types of interactions with the LYS198, HIS215, HIS381, GLN390, and THR391 active sites. Figure 8 shows the two-dimensional poses of **BF4** and **BF7** with the hTYRP1 enzyme.

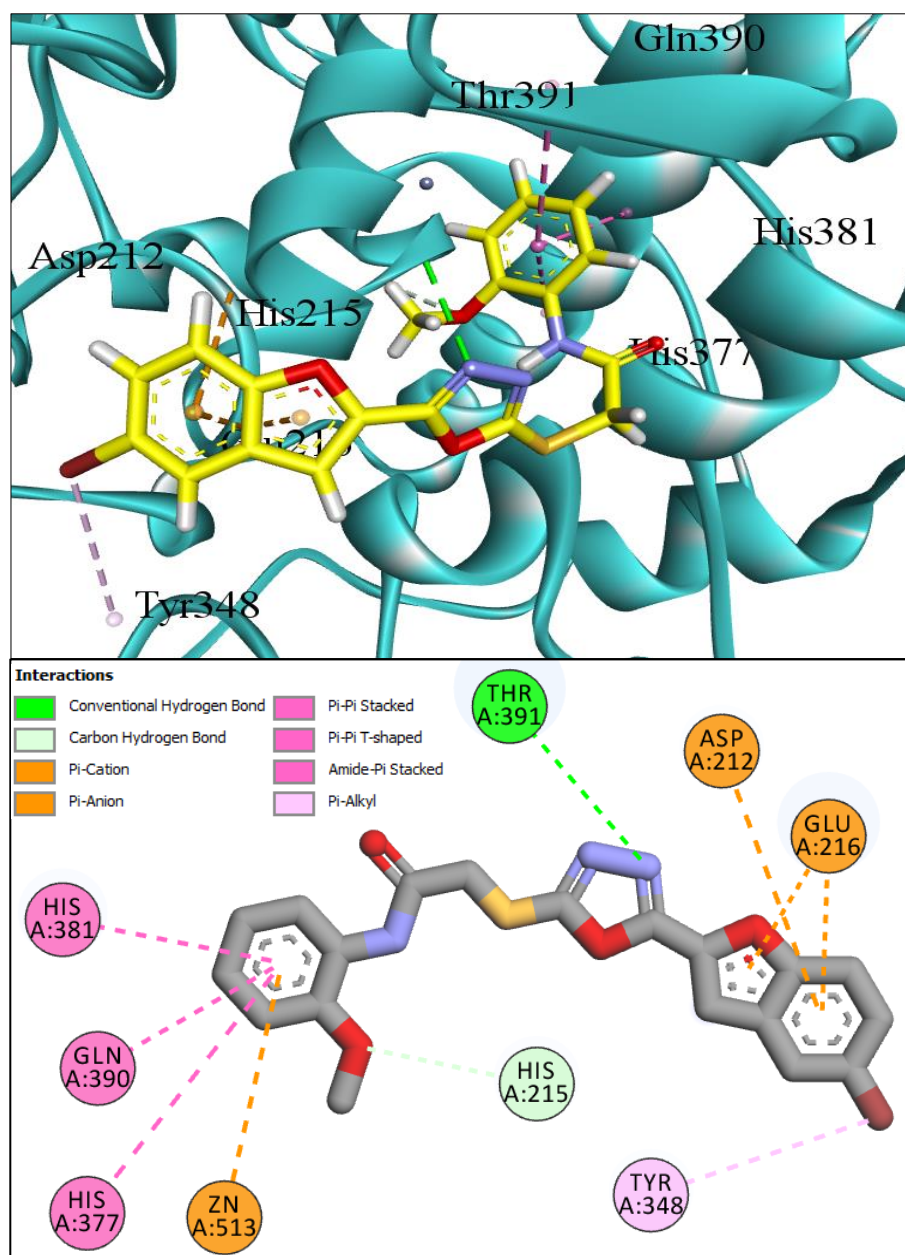


Figure 7. Three-dimensional conformational pose of **BF5** with human tyrosinase-related protein-1 (hTYRP1) (**Upper panel**) and its two-dimensional pose (**Lower panel**).

The binding affinities of the biologically active furan-1,3,4-oxadiazole compounds against hTYR and hTYRP1 are shown in Table 1.

Table 1. Binding affinities of the best binding compounds with the hTyrosinase and hTYRP1 enzymes.

Compound	Binding Affinity in (Kcal/mol) with hTYRP1	Binding Affinity in (Kcal/mol) with hTYR
BF4	−11.50 Kcal/mol	–
BF5	−11.55 Kcal/mol	−13.30 Kcal/mol
BF7	−11.29 Kcal/mol	−11.19 Kcal/mol
BF15	–	−11.88 Kcal/mol
Kojic acid (Standard)	−8.90 Kcal/mol	−6.62 Kcal/mol

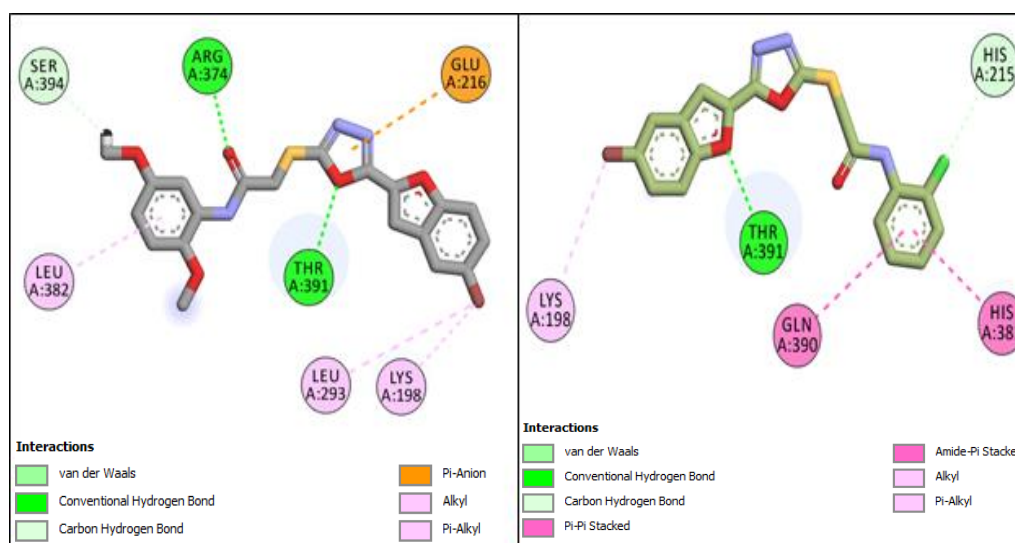


Figure 8. Two-dimensional conformational pose of **BF4** with hTYRP1 (**Left panel**) and two-dimensional conformational pose of **BF7** with hTYRP1 (**Right panel**).

2.2. ADMET and Drug-Likeness Predictive Studies

The pharmacokinetics, or, in short, the ADMET studies along with the drug-likeness in silico investigations, showed that the furan-1,3,4-oxadiazole compounds have significantly good GI-Tract absorption values and they were listed as HIA+. These compounds were listed to have acceptable lipophilic (iLogP) properties and also had good water solubility (LogS-ESOL) values. They were non-inhibitors of the P-gp protein and non-substrates of the CYP450-3A4 enzyme. They were non-inhibitors of renal (OCTs) and were found to be non-AMES toxic. Along with these good ADMET properties, these compounds also showed good medicinal chemistry profiles and accepted the Lipinski rule, Pfizer rule and Golden triangle rule. Table 2 has the different pharmacokinetic properties listed, while Table 3 contains the medicinal chemistry profiles of the best lead compounds identified in this investigation.

Table 2. ADMET profile of **BF4**, **BF5**, **BF7** and **BF15** furan-1,3,4-oxadiazole compounds.

Compounds	HIA+ Values	Lipophilicity (iLogP)	CYP450 3A4 Inhibitor/Substrate	Water Solubility	P-gp Substrate	Carcinogenicity	Renal (OCTs)
BF4	1.0	3.99	Substrate	Moderately soluble	No	None	Non Inhibitor
BF5	1.0	3.75	Substrate	Moderately soluble	No	None	Non Inhibitor
BF7	1.0	3.66	Substrate	Poorly soluble	No	None	Non Inhibitor
BF15	1.0	3.57	Substrate	Moderately soluble	No	None	Non Inhibitor

Table 3. Drug-likeness profile of **BF4**, **BF5**, **BF7** and **BF15** furan-1,3,4-oxadiazole compounds.

Compounds	Bioavailability Score	PAINS Alerts	Brenk Alerts	Lipinski Rule	Pfizer Rule	Golden Triangle Rule	TPSA
BF4	0.55	None	None	Accepted	Accepted	Accepted	124.92 Å ²
BF5	0.55	None	None	Accepted	Accepted	Accepted	115.69 Å ²
BF7	0.55	None	None	Accepted	Accepted	Accepted	106.46 Å ²
BF15	0.55	None	None	Accepted	Accepted	Accepted	106.46 Å ²

2.3. Molecular Dynamics Stability Analysis of the Ligand-Protein Complexes

All atoms' molecular dynamic simulations were conducted for complexes in order to understand and interpret intermolecular dynamics and the stability of docked molecules with the receptor enzymes. As a bio-molecule function in dynamics inside the cells, it is important to evaluate the dynamic behavior rather than focusing on static nature. The trajectories of simulations were generated using the root mean square deviation (RMSD) statistical parameter. RMSD measure the all-atom carbon alpha mean deviation with respect to initial reference position versus time. Higher RMSD describes more structure deviations, while lower RMSD points to small structure changes. The RMSD plot for each complex is provided in Figure 9. The **BF4**-hTYRP1 (mean RMSD of 0.98 Å), **BF15** + hTYR (mean RMSD of 1.62 Å), **BF5** + hTYR (mean RMSD of 0.88 Å) and **BF7** + hTYRP1 (mean RMSD of 1.86 Å) were the most stable complexes that showed little structure deviations in the simulated time. The mean RMSD of these complexes was 1.2 Å. This stable nature of complexes enables the receptors' 3D structure to remain confined and fixed in the presence of compounds during simulation time. The **BF5** + hTYRP1, on the other hand, reported the highest RMSD, which touches almost five angstroms. It is very clear in the analysis that all complexes, after initial small deviation, attained considerable structure stability. The data showed that the compounds are stably docked inside the active pocket of enzymes, and the binding conformation, except for a few initial small adaptations, remained stable throughout the length of simulation time.

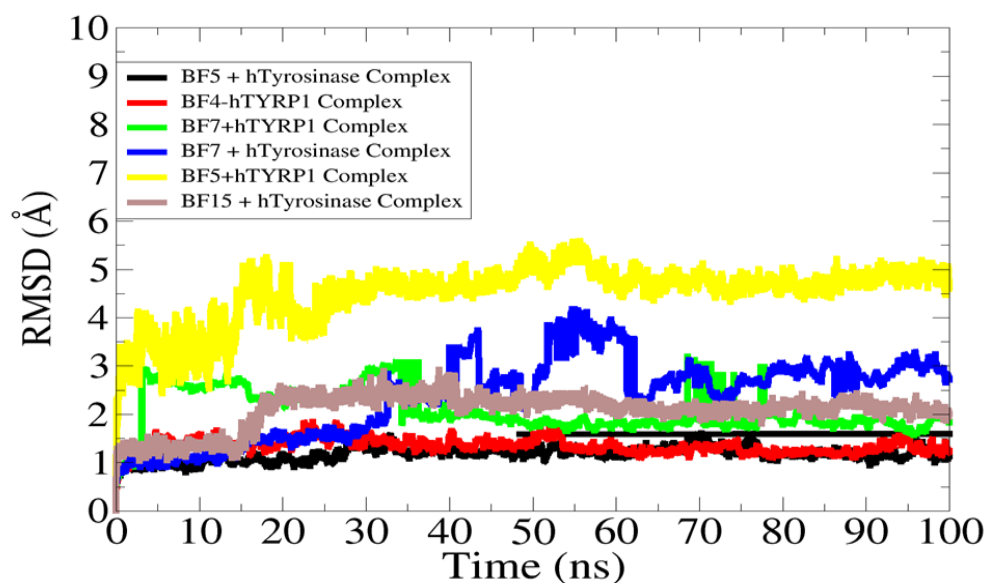


Figure 9. RMSD analysis of complexes to decipher their dynamic stability.

To obtain a further understanding of the residue level flexibility, root mean square fluctuation (RMSF) analysis was conducted. The mean RMSF of BF5 + hTyrosinase, BF7 + hTyrosinase, BF15 + hTyrosinase, BF4-hTYRP1, BF5 + hTYRP1, and BF7 + hTYRP1 is 1.1 Å, 2.2 Å, 0.8 Å, 1.8 Å, 2.7 Å, and 2.9 Å, respectively. All the systems reported stable fluctuations at the residue level with major deviations seen at loops. The RMSF of the complexes is shown in Figure 10.

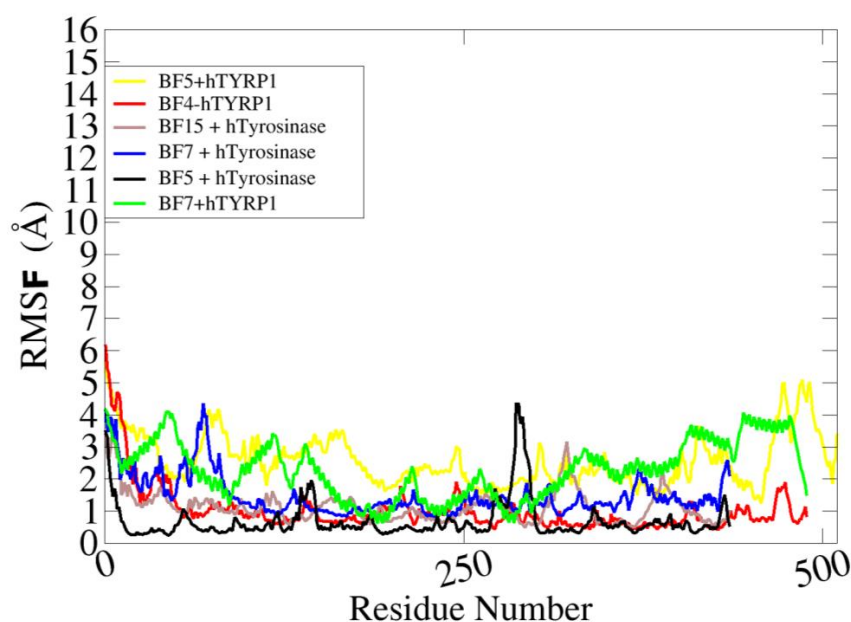


Figure 10. Residue level fluctuation of complexes.

2.4. MM-GBSA/MM-PBSA Binding Free Energy Analysis of Complexes

The binding free energies calculation using MMGBSA and MMPBSA is a significant approach to revalidate the docking results, as they are more reliable and use modest computational power. The order of complexes based on stable net-binding energy is in the following order: **BF4-hTYRP1** > **BF4-hTYRP1** > **BF7 + hTYRP1** > **BF5 + hTYR** > **BF7 + hTYR** > **BF5 + hTYRP1**. Generally, the gas phase energy in all complexes was found to dominate the chemical interaction network between the docked molecules and enzymes' active pocket residues. Decomposing the gas phase energy, the van der Waals energy component was the most dominating, ranging from -55.01 kcal/mol for **BF4-hTYRP1** and -48.62 kcal/mol for **BF5 + hTYRP1**. In addition to that, electrostatic energy played a major role in intermolecular complex formation. The highest contribution was seen in the case of -31.74 kcal/mol for **BF4-hTYRP1** and the lowest contribution was seen in the case of -22.17 kcal/mol for **BF5 + hTYRP1**. The non-favorable contribution was reported from solvation energy, which was highest at 28.99 kcal/mol in **BF5 + hTYR** and lowest at 23.59 kcal/mol in **BF7 + hTYRP1**. The net-binding energy along with each energy parameter value (kcal/mol) is shown in Table 4.

Table 4. Different energy contribution to net binding energy of complexes.

Energy Parameter	BF5 + hTYR (SD)	BF7 + hTYR (SD)	BF15 + hTYR (SD)	BF4-hTYRP1 (SD)	BF5 + hTYRP1 (SD)	BF7 + hTYRP1 (SD)
MM-GBSA						
Van der Waals	-52.20(4.25)	-50.28 (3.68)	-52.62 (5.72)	-55.01 (5.07)	-48.62 (4.68)	-49.55 (5.21)
Electrostatic	-23.89(3.65)	-24.01 (3.56)	-28.21 (2.51)	-31.74 (4.68)	-22.17 (3.66)	-26.30 (4.22)
Delta G gas	-76.09(6.84)	-74.29 (5.38)	-80.83 (8.60)	-86.75 (6.81)	-70.79 (7.25)	-75.85 (6.38)
Delta G solv	28.99 (2.38)	27.68 (7.48)	24.86 (3.84)	25.08 (4.29)	28.64 (4.21)	23.59 (3.56)
Delta Total	-47.1 (5.52)	-46.61 (6.87)	-55.97 (5.69)	-61.67 (6.31)	-42.15 (6.11)	-52.26 (3.98)
MM-PBSA						
Van der Waals	-52.20(4.25)	-50.28 (3.68)	-52.62 (5.72)	-55.01 (5.07)	-48.62 (4.68)	-49.55 (5.21)
Electrostatic	-23.89(4.25)	-24.01 (3.56)	-28.21 (2.51)	-31.74 (4.68)	-22.17 (3.66)	-26.30 (4.22)
Delta G gas	-76.09(6.84)	-74.29 (5.38)	-80.83 (8.60)	-86.75 (6.81)	-70.79 (7.25)	-75.85 (6.38)
Delta G solv	25.60 (1.68)	25.07 (2.58)	28.61 (3.64)	24.01 (3.29)	27.64 (4.62)	24.50 (3.33)
Delta Total	-50.49(4.68)	-49.22 (5.28)	-52.22 (4.22)	-62.74 (2.67)	-43.15 (3.08)	-51.35 (2.67)

3. Material and Methods

3.1. Structures of Synthesized Furan-1,3,4-Oxadiazoles BF1–BF16

The structures of furan-1,3,4-oxadiazole structural motifs, which were synthesized by Irfan, A et al. [38,39], are shown in Table 5.

Table 5. Structures of synthetic furan-1,3,4-oxadiazoles BF1–BF16.

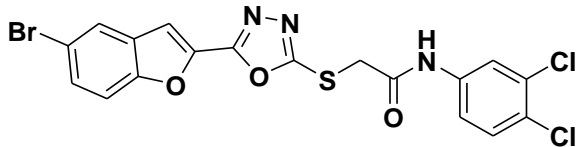
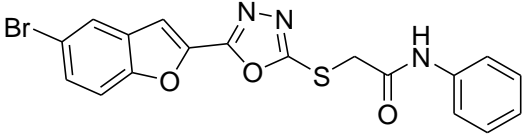
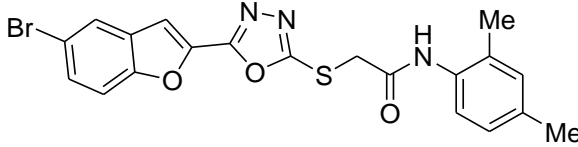
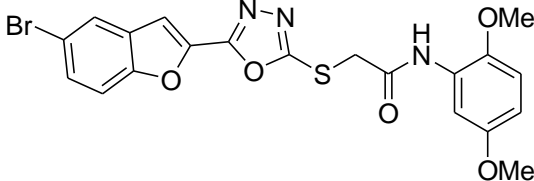
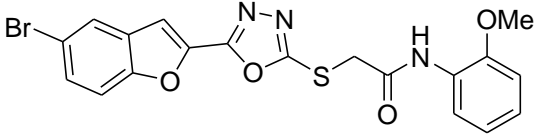
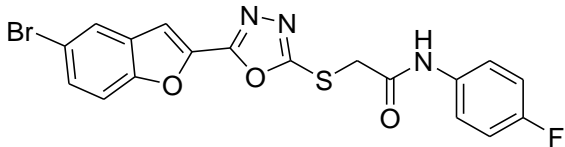
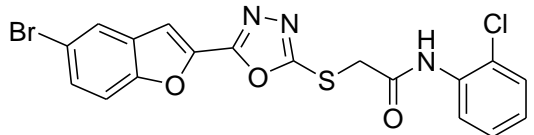
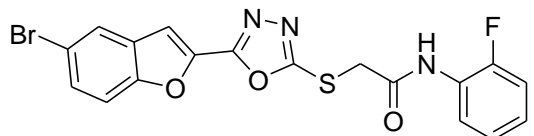
Compounds	Structures of Furan-1,3,4-Oxadiazssoles
BF1	
BF2	
BF3	
BF4	
BF5	
BF6	
BF7	
BF8	

Table 5. Cont.

Compounds	Structures of Furan-1,3,4-Oxadiazsoles
BF9	
BF10	
BF11	
BF12	
BF13	
BF14	
BF15	
BF16	

3.2. In Silico Biological Evaluation of Furan-1,3,4-Oxadiazoles BF1–BF16

3.2.1. Molecular Docking, ADME&T, Drug-Likeness, and Protein Homology Modeling Studies

The PDB structure of the target enzyme hTYR was predicted with homology modeling via the Swiss-Model prediction server using the fasta sequence of human tyrosinase with Uniprot ID = P14679 (because its resolved crystal structure is not available yet), while the structure of the hTYRP1 PDB ID-5M8M was accessed from the RCSB website for the computational investigations. The molecular docking investigations were performed via the Molecular Operating Environment (MOE) (Version-2009.10). Before docking, the protein structure of the hTYR and hTYRP1 enzyme was prepared for docking studies

using the Biovia DS software. The structures of ligands **BF1–BF16** were prepared using the ChemDraw Professional. The (.mol) format structure of these ligands was imported into MOE, where the partial charges were added to them along with energy minimization of these compounds, which was performed using the MMFF94x –ff. In MOE, the protein structures were loaded and 3D-protonated; after that, its site-finder function was utilized for the active site identification. The triangle matcher technique and the London-dG scoring functions were used for the binding affinity estimations of these compounds against the target enzymes by the DOCK module of the MOE Software. Furthermore, the BIOVIA DS (Version-2017) software was utilized for the interaction analysis and visualization of the ligand–protein complexes [40–49]. The ADMET and drug-likeness investigation were carried out using the Swissadme and ADMETlab (Version 2.0) online servers, while the admetSAR (Version 1.0 and 2.0) online servers were utilized for the toxicity investigations of these compounds [50–53].

3.2.2. Molecular Dynamic Simulation Studies

For all docked complexes, the computer-based molecular dynamic simulations were performed employing AMBER (Version-20) simulation software. This analysis was important to conduct in order to understand protein–ligand’s stability and dynamics in simulated time scale. In order to define parameters for the proteins and compounds, AMBER FF14SB and GAFF force fields were used, respectively. Charge assignment was carried out using the AMBER antechamber program. The placement of complexes into TIP3 simulation box was then accomplished by setting the distance between the molecules and box edge as 12 Å. Addition of counter ions was performed to obtain neutral systems. Long-range electrostatic interactions were evaluated using the Ewald summation method. The SHAKE algorithm was applied to constrain bounded hydrogen atoms, while to control temperature and pressure, Langevin and Berendsen’s barostats were run, respectively [54–60].

Prior to production, the complexes were minimized for energy in two stages; first by fast steepest descent for 10,000 steps followed by slow conjugate gradient for 15,000 steps. The complexes were then heated to 300 K. The equilibration of complexes was achieved using NPT and NVE ensembles with a collision frequency of 2. The production run was performed for 100 ns and the generated trajectories were evaluated through the CPPTRAJ tool [61]. The statistical plots were produced using XMGRACE (Version-5.1).

3.2.3. Estimation of Binding Energies and Interactions (MM-GBSA and MM-PBSA)

Estimation of binding interactions was carried out using the molecular mechanics Poisson–Boltzmann surface area (MM-PBSA) technique of AMBER (Version-20). This involves the calculation of continuum electrostatics, molecular mechanics, and solvent-accessible surface area [62,63]. Equation (1) was used for this calculation to describe the difference between the energy of the complex, receptor and ligand, as shown below (Equation (1)) [64,65].

$$\Delta G_{\text{bind}} = G_{\text{complex}} - G_{\text{protein}} - G_{\text{ligand}} = \Delta E_{\text{MM}} + \Delta G_{\text{sol}} - T\Delta S \quad (1)$$

The equation was performed on 1000 simulation frames and the net-binding energies were estimated as a sum of gas phase and solvation energies.

4. Conclusions

In conclusion, we have evaluated sixteen furan-1,3,4-oxadiazole tethered *N*-phenylacetamides, **BF1–BF16**, which were evaluated via in silico analysis for melanogenesis. We have screened out the most bioactive *N*-phenylacetamide-based furan-1,3,4-oxadiazole scaffolds, **BF4** and **BF5**, against hTYRP1 and hTYR, respectively. Among these promising molecules, 2,5-dimethoxy containing furan-1,3,4-oxadiazole, **BF4**, displayed stronger binding affinity (–11.50 kcal/mol) against hTYRP1, and 2-methoxy containing furan-1,3,4-oxadiazole, **BF5**, exhibited the best binding affinity (–13.30 kcal/mol) against

hTYR compared to the binding in affinities of its standard inhibitor drug kojic acid. Furthermore, the MM-GBSA/MM-PBSA binding energy analysis also showed that these two compounds, **BF4** and **BF5**, bind strongly with the target enzymes hTYRP1 and hTYR. The molecular dynamics simulations stability analysis of the simulation trajectories of these complexes after the 100 ns simulation time provided insights into the stable bindings of these *N*-phenylacetamide-based furan-1,3,4-oxadiazole compounds (**BF4** and **BF5**) within the hTYRP1 and hTYR enzymes active sites. The furan-1,3,4-oxadiazole tethered *N*-phenylacetamide structural hybrids **BF4** and **BF5** also exhibited good ADMET and drug-likeness properties, which suggests the suitability of these compounds as potent inhibitory drug candidates against hTYRP1 and hTYR.

Author Contributions: Conceptualization, A.F.Z., M.E.A.Z. and A.I.; methodology, A.I.; software, S.F., A.I. and S.A.; validation, S.F., S.A. and A.I.; formal analysis, A.I., S.F., S.J. and S.A.; investigation, A.I. and S.F.; resources, A.F.Z. and S.A.A.-H.; data curation, S.A.A.-H., A.I. and S.J.; writing—original draft preparation, A.I.; writing—review and editing, A.I., B.P., S.F., A.F.Z. and M.E.A.Z.; visualization, S.F.; supervision, A.F.Z.; project administration, A.F.Z. and M.E.A.Z.; funding acquisition, S.A.A.-H. and M.E.A.Z. All authors have read and agreed to the published version of the manuscript.

Funding: This research was supported by the Deanship of Scientific Research, Imam Mohammad Ibn Saud Islamic University (IMSIU), Saudi Arabia.

Institutional Review Board Statement: Not applicable.

Informed Consent Statement: Not applicable.

Data Availability Statement: Data is contained within the article.

Acknowledgments: The authors acknowledge the Government College University Faisalabad for the research facilities provided to carry out this research work.

Conflicts of Interest: The authors declare no conflict of interest.

References

- Zhang, W.; Zeng, W.; Jiang, A.; He, Z.; Shen, X.; Dong, X.; Feng, J.; Lu, H. Global, Regional and National Incidence, Mortality and Disability-Adjusted Life-Years of Skin Cancers and Trend Analysis from 1990 to 2019: An Analysis of the Global Burden of Disease Study 2019. *Cancer Med.* **2021**, *10*, 4905–4922. [[CrossRef](#)] [[PubMed](#)]
- Ijaz, S.; Akhtar, N.; Khan, M.S.; Hameed, A.; Irfan, M.; Arshad, M.A.; Ali, S.; Asrar, M. Plant Derived Anticancer Agents: A Green Approach towards Skin Cancers. *Biomed. Pharmacother.* **2018**, *103*, 1643–1651. [[CrossRef](#)] [[PubMed](#)]
- Apalla, Z.; Lallas, A.; Sotiriou, E.; Lazaridou, E.; Ioannides, D. Epidemiological Trends in Skin Cancer. *Dermatol. Pract. Concept.* **2017**, *7*, 1–6. [[CrossRef](#)] [[PubMed](#)]
- Simões, M.C.F.; Sousa, J.J.S.; Pais, A.A.C.C. Skin Cancer and New Treatment Perspectives: A Review. *Cancer Lett.* **2015**, *357*, 8–42. [[CrossRef](#)]
- Chummun, S.; McLean, N.R. The Management of Malignant Skin Cancers. *Surgery* **2017**, *35*, 519–524.
- Testori, A.; Rutkowski, P.; Marsden, J.; Bastholt, L.; Chiarion-Sileni, V.; Hauschild, A.; Eggermont, A.M.M. Surgery and Radiotherapy in the Treatment of Cutaneous Melanoma. *Ann. Oncol.* **2009**, *20*, vi22–vi29. [[CrossRef](#)]
- Shtivelman, E.; Davies, M.A.; Hwu, P.; Yang, J.; Lotem, M.; Oren, M.; Flaherty, K.T.; Fisher, D.E. Pathways and Therapeutic Targets in Melanoma. *Oncotarget* **2014**, *5*, 1701–1752. [[CrossRef](#)]
- Gray-Schopfer, V.; Wellbrock, C.; Marais, R. Melanoma Biology and New Targeted Therapy. *Nature* **2007**, *445*, 851–857. [[CrossRef](#)]
- Xu, X.; Zhang, P.J.; Elder, D.E.; Haupt, H.M.; Stern, J.B.; Multhaupt, H.A.B. Tyrosinase Expression in Malignant Melanoma, Desmoplastic Melanoma, and Peripheral Nerve Tumors. *Arch. Pathol. Lab. Med.* **2003**, *127*, 1083–1085. [[CrossRef](#)]
- Bandarchi, B.; Ma, L.; Navab, R.; Seth, A.; Rasty, G. From Melanocyte to Metastatic Malignant Melanoma. *Dermatol. Res. Pract.* **2010**, *2010*, 583748. [[CrossRef](#)]
- Kobayashi, T.; Urabe, K.; Winder, A.; Jiménez-Cervantes, C.; Imokawa, G.; Brewington, T.; Solano, F.; García-Borrón, J.C.; Hearing, V.J. Tyrosinase Related Protein 1 (TRP1) Functions as a DHICA Oxidase in Melanin Biosynthesis. *EMBO J.* **1994**, *13*, 5818–5825. [[CrossRef](#)]
- Ghanem, G.; Fabrice, J. Tyrosinase Related Protein 1 (TYRP1/Gp75) in Human Cutaneous Melanoma. *Mol. Oncol.* **2011**, *5*, 150–155. [[CrossRef](#)] [[PubMed](#)]
- Khalil, D.N.; Postow, M.A.; Ibrahim, N.; Ludwig, D.L.; Cosaert, J.; Kambhampati, S.R.P.; Tang, S.; Grebennik, D.; Kauh, J.S.W.; Lenz, H.J.; et al. An Open-Label, Dose-Escalation Phase I Study of Anti-TYRP1 Monoclonal Antibody IMC-20D7S for Patients with Relapsed or Refractory Melanoma. *Clin. Cancer Res.* **2016**, *22*, 5204–5210. [[CrossRef](#)] [[PubMed](#)]

14. Buitrago, E.; Hardré, R.; Haudecoeur, R.; Jamet, H.; Belle, C.; Boumendjel, A.; Bubacco, L.; Réglie, M. Are Human Tyrosinase and Related Proteins Suitable Targets for Melanoma Therapy? *Curr. Top. Med. Chem.* **2016**, *16*, 3033–3047. [[CrossRef](#)]
15. Mroz, P.; Huang, Y.; Szokalska, A.; Zhiyentayev, T.; Janjua, S.; Nifli, A.; Sherwood, M.E.; Ruzié, C.; Borbas, K.E.; Fan, D.; et al. Stable Synthetic Bacteriochlorins Overcome the Resistance of Melanoma to Photodynamic Therapy. *FASEB J.* **2010**, *24*, 3160–3170. [[CrossRef](#)] [[PubMed](#)]
16. Kameyama, K.; Sakai, C.; Kuge, S.; Nishiyama, S.; Tomita, Y.; Ito, S.; Wakamatsu, K.; Hearing, V.J. The Expression of Tyrosinase, Tyrosinase-Related Proteins 1 and 2 (TRP1 and TRP2), the Silver Protein, and a Melanogenic Inhibitor in Human Melanoma Cells of Differing Melanogenic Activities. *Pigment. Cell Res.* **1995**, *8*, 97–104. [[CrossRef](#)] [[PubMed](#)]
17. Brozyna, A.A.; VanMiddlesworth, L.; Slominski, A.T. Inhibition of Melanogenesis as a Radiation Sensitizer for Melanoma Therapy. *Int. J. Cancer* **2008**, *123*, 1448–1456. [[CrossRef](#)]
18. Sharma, K.V.; Bowers, N.; Davids, L.M. Photodynamic Therapy-Induced Killing Is Enhanced in Depigmented Metastatic Melanoma Cells. *Cell Biol. Int.* **2011**, *35*, 939–944. [[CrossRef](#)]
19. Yan, J.; Tingey, C.; Lyde, R.; Gorham, T.C.; Choo, D.K.; Muthumani, A.; Myles, D.; Weiner, L.P.; Kraynyak, K.A.; Reuschel, E.L.; et al. Novel and Enhanced Anti-Melanoma DNA Vaccine Targeting the Tyrosinase Protein Inhibits Myeloid-Derived Suppressor Cells and Tumor Growth in a Syngeneic Prophylactic and Therapeutic Murine Model. *Cancer Gene Ther.* **2014**, *21*, 507–517. [[CrossRef](#)]
20. Vargas, A.J.; Sittadjody, S.; Thangasamy, T.; Mendoza, E.E.; Limesand, K.H.; Burd, R. Exploiting Tyrosinase Expression and Activity in Melanocytic Tumors: Quercetin and the Central Role of P53. *Integr. Cancer Ther.* **2011**, *10*, 328–340. [[CrossRef](#)]
21. Jawaid, S.; Khan, T.H.; Osborn, H.M.I.; Williams, N.A.O. Tyrosinase Activated Melanoma Prodrugs. *Anticancer Agents Med. Chem.* **2012**, *9*, 717–727. [[CrossRef](#)] [[PubMed](#)]
22. Dean, F.M.; Sargent, M.V. 3,10-Furans and their Benzo Derivatives: (i) Structure. In *Comprehensive Heterocyclic Chemistry*; Elsevier: Amsterdam, The Netherlands, 1984; Volume 4, pp. 531–597. [[CrossRef](#)]
23. Rymbai, E.M.; Chakraborty, A.; Choudhury, R.; Biplab De, N.V. Review on Chemistry and Therapeutic Activity of the Derivatives of Furan and Oxazole: The Oxygen Containing Heterocycles. *Der Pharma Chem.* **2019**, *11*, 20–41.
24. Rodd, E.H. *Chemistry of Carbon Compounds: A Modern Comprehensive Treatise*; Elsevier: Amsterdam, The Netherlands, 1971.
25. Limpricht, H. Ueber das Tetraphenol C₄H₄O. *Ber. Der Dtsch. Chem. Ges.* **1870**, *3*, 90–91. [[CrossRef](#)]
26. Miao, Y.H.; Hu, Y.H.; Yang, J.; Liu, T.; Sun, J.; Wang, X.J. Natural source, bioactivity and synthesis of benzofuran derivatives. *RSC Adv.* **2019**, *9*, 27510. [[CrossRef](#)] [[PubMed](#)]
27. Vanjare, B.D.; Choi, N.G.; Mahajan, P.G.; Raza, H.; Hassan, M.; Han, Y.; Yu, S.M.; Kim, S.J.; Seo, S.Y.; Lee, K.H. Novel 1,3,4-oxadiazole compounds inhibit the tyrosinase and melanin level: Synthesis, in-vitro, and in-silico studies. *Bioorg. Med. Chem.* **2021**, *1*, 116222. [[CrossRef](#)]
28. Mann, T.; Gerwat, W.; Batzer, J.; Eggers, K.; Scherner, C.; Wenck, H.; Stäb, F.; Hearing, V.J.; Röhm, K.H.; Kolbe, L. Inhibition of Human Tyrosinase Requires Molecular Motifs Distinctively Different from Mushroom Tyrosinase. *J. Investig. Dermatol.* **2018**, *138*, 1601–1608. [[CrossRef](#)]
29. Roulier, B.; Pérès, B.; Haudecoeur, R. Advances in the Design of Genuine Human Tyrosinase Inhibitors for Targeting Melanogenesis and Related Pigmentations. *J. Med. Chem.* **2020**, *63*, 13428–13443. [[CrossRef](#)]
30. Koirala, P.; Seong, S.H.; Zhou, Y.; Shrestha, S.; Jung, H.A.; Choi, J.S. Structure–Activity Relationship of the Tyrosinase Inhibitors Kuwanon G, Mulberrofuran G, and Albanol B from Morus Species: A Kinetics and Molecular Docking Study. *Molecules* **2018**, *23*, 1413. [[CrossRef](#)]
31. Okombi, S.; Rival, D.; Bonnet, S.; Mariotte, A.M.; Perrier, E.; Boumendjel, A. Discovery of Benzylidenebenzofuran-3(2H)-One (Aurones) as Inhibitors of Tyrosinase Derived from Human Melanocytes. *J. Med. Chem.* **2006**, *49*, 329–333. [[CrossRef](#)]
32. Hu, X.; Wang, M.; Yan, G.R.; Yu, M.H.; Wang, H.Y.; Hou, A.J. 2-Arylbzofuran and Tyrosinase Inhibitory Constituents of Morus Notabilis. *J. Asian Nat. Prod. Res.* **2012**, *14*, 1103–1108. [[CrossRef](#)]
33. Faiz, S.; Zahoor, A.F.; Ajmal, M.; Kamal, S.; Ahmad, S.; Abdelgawad, A.M.; Elnaggar, E.M. Design, synthesis, antimicrobial evaluation, and laccase catalysis effect of novel benzofuran–oxadiazole and benzofuran–triazole hybrids. *J. Heterocycl. Chem.* **2019**, *56*, 2839–2852. [[CrossRef](#)]
34. Hassan, M.; Ashraf, Z.; Abbas, Q.; Raza, H.; Seo, S.Y. Exploration of Novel Human Tyrosinase Inhibitors by Molecular Modeling, Docking and Simulation Studies. *Interdiscip. Sci. Comput. Life Sci.* **2018**, *10*, 68–80. [[CrossRef](#)] [[PubMed](#)]
35. Shahzadi, I.; Zahoor, F.A.; Rasul, A.; Mansha, A.; Ahmad, S.; Raza, Z. Synthesis, hemolytic studies, and in silico modeling of novel acefylline-1,2,4-triazole hybrids as potential anti-cancer agents against MCF-7 and A549. *ACS Omega* **2021**, *6*, 11943–11953. [[CrossRef](#)] [[PubMed](#)]
36. Lee, J.H.; Mei, H.C.; Kuo, I.C.; Lee, T.H.; Chen, Y.H.; Lee, C.K. Characterizing Tyrosinase Modulators from the Roots of Angelica Keiskei Using Tyrosinase Inhibition Assay and UPLC-MS/MS as the Combinatorial Novel Approach. *Molecules* **2019**, *24*, 3297. [[CrossRef](#)] [[PubMed](#)]
37. Waterhouse, A.; Bertoni, M.; Bienert, S.; Studer, G.; Tauriello, G.; Gumienny, R.; Heer, F.T.; De Beer, T.A.P.; Rempfer, C.; Bordoli, L.; et al. SWISS-MODEL: Homology Modelling of Protein Structures and Complexes. *Nucleic Acids Res.* **2018**, *46*, W296–W303. [[CrossRef](#)]

38. Irfan, A.; Zahoor, A.F.; Kamal, S.; Hassan, M.; Kloczkowski, A. Ultrasonic-Assisted Synthesis of Benzofuran Appended Oxadiazole Molecules as Tyrosinase Inhibitors: Mechanistic Approach through Enzyme Inhibition, Molecular Docking, Chemoinformatics, ADMET and Drug-Likeness Studies. *Int. J. Mol. Sci.* **2022**, *23*, 10979. [[CrossRef](#)]
39. Irfan, A.; Faiz, S.; Rasul, A.; Zafar, R.; Zahoor, A.F.; Kotwica-Mojzzych, K.; Mojzzych, M. Exploring the Synergistic Anticancer Potential of Benzofuran–Oxadiazoles and Triazoles: Improved Ultrasound- and Microwave-Assisted Synthesis, Molecular Docking, Hemolytic, Thrombolytic and Anticancer Evaluation of Furan-Based Molecules. *Molecules* **2022**, *27*, 1023. [[CrossRef](#)]
40. Lai, X.; Wichers, H.J.; Soler-Lopez, M.; Dijkstra, B.W. Structure of Human Tyrosinase Related Protein 1 Reveals a Binuclear Zinc Active Site Important for Melanogenesis. *Angew. Chem.* **2017**, *129*, 9944–9947. [[CrossRef](#)]
41. Burley, S.K.; Berman, H.M.; Bhikadiya, C.; Bi, C.; Chen, L.; Di Costanzo, L.; Christie, C.; Dalenberg, K.; Duarte, J.M.; Dutta, S.; et al. RCSB Protein Data Bank: Biological Macromolecular Structures Enabling Research and Education in Fundamental Biology, Biomedicine, Biotechnology and Energy. *Nucleic Acids Res.* **2019**, *47*, D464–D474. [[CrossRef](#)]
42. Vilar, S.; Cozza, G.; Moro, S. Medicinal Chemistry and the Molecular Operating Environment (MOE): Application of QSAR and Molecular Docking to Drug Discovery. *Curr. Top. Med. Chem.* **2008**, *8*, 1555–1572. [[CrossRef](#)]
43. Faisal, S.; Lal Badshah, S.; Kubra, B.; Sharaf, M.; Emwas, A.H.; Jaremko, M.; Abdalla, M. Computational Study of Sars-Cov-2 Rna Dependent Rna Polymerase Allosteric Site Inhibition. *Molecules* **2022**, *27*, 223. [[CrossRef](#)] [[PubMed](#)]
44. Dassault Systèmes. *BIOVIA Discovery Studio Visualizer, Release 2017*; Dassault Systèmes: Vélizy-Villacoublay, France, 2023.
45. Mills, N. ChemDraw Ultra 10.0 CambridgeSoft, 100 CambridgePark Drive, Cambridge, MA 02140. www.cambridgesoft.com. Commercial Price: \$1910 for download, \$2150 for CD-ROM; Academic Price: \$710 for download, \$800 for CD-ROM. *J. Am. Chem. Soc.* **2006**, *128*, 13649–13650. [[CrossRef](#)]
46. Shinu, P.; Sharma, M.; Gupta, G.L.; Mujwar, S.; Kandeel, M.; Kumar, M.; Nair, A.B.; Goyal, M.; Singh, P.; Attimarad, M.; et al. Computational Design, Synthesis, and Pharmacological Evaluation of Naproxen-Guaiacol Chimera for Gastro-Sparing Anti-Inflammatory Response by Selective COX2 Inhibition. *Molecules* **2022**, *27*, 6905. [[CrossRef](#)] [[PubMed](#)]
47. Mujwar, S.; Sun, L.; Fidan, O. In silico evaluation of food-derived carotenoids against SARS-CoV-2 drug targets: Crocin is a promising dietary supplement candidate for COVID-19. *J. Food Biochem.* **2022**, *46*, e14219. [[CrossRef](#)] [[PubMed](#)]
48. Fidan, O.; Mujwar, S.; Kciuk, M. Discovery of adapalene and dihydrotachysterol as antiviral agents for the Omicron variant of SARS-CoV-2 through computational drug repurposing. *Mol. Divers.* **2022**, *4*, 1–13. [[CrossRef](#)]
49. Kciuk, M.; Mujwar, S.; Szymanowska, A.; Marciniak, B.; Bukowski, K.; Mojzzych, M.; Kontek, R. Preparation of Novel Pyrazolo[4,3-*e*]tetrazolo[1,5-*b*][1,2,4]triazine Sulfonamides and Their Experimental and Computational Biological Studies. *Int. J. Mol. Sci.* **2022**, *23*, 5892. [[CrossRef](#)] [[PubMed](#)]
50. Daina, A.; Michielin, O.; Zoete, V. SwissADME: A Free Web Tool to Evaluate Pharmacokinetics, Drug-Likeness and Medicinal Chemistry Friendliness of Small Molecules. *Sci. Rep.* **2017**, *7*, 42717. [[CrossRef](#)]
51. Xiong, G.; Wu, Z.; Yi, J.; Fu, L.; Yang, Z.; Hsieh, C.; Yin, M.; Zeng, X.; Wu, C.; Lu, A.; et al. ADMETlab 2.0: An Integrated Online Platform for Accurate and Comprehensive Predictions of ADMET Properties. *Nucleic Acids Res.* **2021**, *49*, W5–W14. [[CrossRef](#)]
52. Yang, H.; Lou, C.; Sun, L.; Li, J.; Cai, Y.; Wang, Z.; Li, W.; Liu, G.; Tang, Y. AdmetSAR 2.0: Web-Service for Prediction and Optimization of Chemical ADMET Properties. *Bioinformatics* **2019**, *35*, 1067–1069. [[CrossRef](#)]
53. Cheng, F.; Li, W.; Zhou, Y.; Shen, J.; Wu, Z.; Liu, G.; Lee, P.W.; Tang, Y. AdmetSAR: A Comprehensive Source and Free Tool for Assessment of Chemical ADMET Properties. *J. Chem. Inf. Model.* **2012**, *52*, 3099–3105. [[CrossRef](#)]
54. Case, D.A.; Cheatham, T.E., III; Darden, T.; Gohlke, H.; Luo, R.; Merz, K.M., Jr.; Onufriev, A.; Simmerling, C.; Wang, B.; Woods, R.J. The Amber Biomolecular Simulation Programs. *J. Comb. Chem.* **2005**, *26*, 1668–1688. [[CrossRef](#)]
55. Maier, J.A.; Martinez, C.; Kasavajhala, K.; Wickstrom, L.; Hauser, K.E.; Simmerling, C. Ff14SB: Improving the Accuracy of Protein Side Chain and Backbone Parameters from Ff99SB. *J. Chem. Theory Comput.* **2015**, *11*, 3696–3713. [[CrossRef](#)] [[PubMed](#)]
56. Wang, J.; Wolf, R.M.; Caldwell, J.W.; Kollman, P.A.; Case, D.A. Development and Testing of a General Amber Force Field. *J. Comput. Chem.* **2004**, *25*, 1157–1174. [[CrossRef](#)] [[PubMed](#)]
57. Wang, J.; Wang, W.; Kollman, P.A.; Case, D.A. Antechamber, An Accessory Software Package For Molecular Mechanical Calculations. *J. Am. Chem. Soc.* **2001**, *222*, 403.
58. Saunders, W.R.; Grant, J.; Müller, E.H. Long Range Forces in a Performance Portable Molecular Dynamics Framework. *Adv. Parallel Comput.* **2018**, *22*, 37–46. [[CrossRef](#)]
59. Paquet, E.; Viktor, H.L. Molecular Dynamics, Monte Carlo Simulations, and Langevin Dynamics: A Computational Review. *BioMed Res. Int.* **2015**, *2015*, 183918. [[CrossRef](#)]
60. Lin, Y.; Pan, D.; Li, J.; Zhang, L.; Shao, X. Application of BerendsenBarostat in Dissipative Particle Dynamics for Nonequilibrium Dynamic Simulation. *J. Chem. Phys.* **2017**, *146*, 124108. [[CrossRef](#)]
61. Roe, D.R.; Cheatham, T.E. PTRAJ and CPPTRAJ: Software for Processing and Analysis of Molecular Dynamics Trajectory Data. *J. Chem. Theory Comput.* **2013**, *9*, 3084–3095. [[CrossRef](#)]
62. Miller, B.R.; McGee, T.D.; Swails, J.M.; Homeyer, N.; Gohlke, H.; Roitberg, A.E. MMPBSA.Py: An Efficient Program for End-State Free Energy Calculations. *J. Chem. Theory Comput.* **2012**, *8*, 3314–3321. [[CrossRef](#)]

63. Sun, H.; Li, Y.; Shen, M.; Tian, S.; Xu, L.; Pan, P.; Guan, Y.; Hou, T. Assessing the Performance of MM/PBSA and MM/GBSA Methods. 5. Improved Docking Performance Using High Solute Dielectric Constant MM/GBSA and MM/PBSA Rescoring. *Phys. Chem. Chem. Phys.* **2014**, *16*, 22035–22045. [[CrossRef](#)]
64. Hou, T.; Wang, J.; Li, Y.; Wang, W. Assessing the Performance of the MM/PBSA and MM/GBSA Methods. 1. The Accuracy of Binding Free Energy Calculations Based on Molecular Dynamics Simulations. *J. Chem. Inf. Model.* **2011**, *51*, 69–82. [[CrossRef](#)] [[PubMed](#)]
65. Zhang, Y.; Qiu, Y.; Zhang, H. Computational Investigation of Structural Basis for Enhanced Binding of Isoflavone Analogues with Mitochondrial Aldehyde Dehydrogenase. *ACS Omega* **2022**, *7*, 8115–8127. [[CrossRef](#)] [[PubMed](#)]

Disclaimer/Publisher's Note: The statements, opinions and data contained in all publications are solely those of the individual author(s) and contributor(s) and not of MDPI and/or the editor(s). MDPI and/or the editor(s) disclaim responsibility for any injury to people or property resulting from any ideas, methods, instructions or products referred to in the content.